ingegneria sismica
International Journal of Earthquake Engineering
Anno XLIII - Num. 1 - 2026

Nitrogen-doped carbon quantum dots as multifunctional interfacial modifiers: simultaneous enhancement of efficiency, stability, and reduction of hysteresis effects in chalcogenide solar cells

Xiaolin Wang[1,*]

[1] School of Materials, Luoyang Institute of Science and Technology, Luoyang, Henan, 471023, China

SUMMARY: *In view of their structural versatility and high photoelectric capabilities, nitrogen-doped carbon quantum dots (N-CQDs) have been observed to exhibit promising potential as functional material for improving the efficiency of chalcogenide-based solar cells. In this work, the fabrication of N-CQDs using fennel seeds was done in a process that involved the steps of drying, grinding, hydrothermal process, filtration, centrifugation, and dialysis. Characterization methods such as UV-Visible spectroscopy, fluorescence spectroscopy, and SEM analysis were used to analyze and assess the uniformity of the produced particles when used as a component of solar cells. As revealed by characterization studies, it was clear that the obtained N-CQDs had a suitable energy-level position and good luminescence capabilities. On inclusion within the charge-transport interface layer of the solar cell, its efficiency improved to 20.34%, and the short-circuit current density rose to 23.94 mA cm^{-2}. Moreover, N-CQDs have the potential to reduce the level of interfacial defects and the complexity of the carriers, hence reducing the hysteresis effect. The hydrophobic nature of the quantum dots prevented moisture penetration and consequently resulted in 51% enhancement of the CQDs stability.*

KEYWORDS: *Chalcogenide solar cells; Nitrogen-doped carbon quantum dots; Ultraviolet-visible absorption spectra; Interface modification; Electrochemical performance*

1 Introduction

The growth of industry and big data have caused an increase in energy consumption. The interest towards chalcogenide perovskite solar cells is considerable as a result of their good energy efficiency, low production costs, and excellent processability [1, 2]. Yet in terms of their practical application, performance depends on a number of aspects, such as defects present in the absorber layer and charge transfer at the interface [3]. The interface, as a transition region between different materials, plays a crucial role in charge transport and collection. If the charge transport at the interface is poor, it will lead to an increase in charge compounding, thus reducing the photoelectric conversion efficiency of the cell [4]. Moreover, vacancies and impurities in the chalcogenide absorber impact carrier transport in the device and its lifetime [5, 6]. For this reason, improving cell performance through interfacial engineering and defect passivation has become a major focus in current research on chalcogenide photovoltaics.

N-CQDs have been suggested as effective multifunctional interfacial modifiers due to their ability to passivate defects, rich surface functionality, and excellent chemical and physical

*18910514927@163.com
https://doi.org/10.65102/is2026181
Published: 30 April, 2026

stability [7-9]. CQDs refer to nanoscale carbon structures that are usually less than 10 nm in size, exhibiting a spherical or quasi-spherical shape and the ability to provide stable luminescence [10]. The unique characteristics of CQDs are attributed to their low toxicity and biocompatibility with up-conversion fluorescence, desirable electrical properties, tunability of surface chemistry, and ease of fabrication [11-13]. When used as multifunctional interfacial modifiers, N-CQDs will be able to passivate surface and grain boundary defects using their surface functional groups. Defect passivation will decrease non-radiative recombination losses, improve efficiency and performance stability, and prevent hysteresis [14-17].

Concerning the role of N-CQDs in improving chalcogenide solar cells, Kırbıyık et al [18] reported an efficient enhancement of defects' passivation, crystal optimization, and non-radiative recombination suppression. The abovementioned characteristics contributed to increasing charge transfer and the final power conversion efficiency in the investigated cells. In their study, Li et al. synthesized N-CQDs using human hair and characterized their multifunctional properties in terms of being added to the interfacial layer of chalcogenides. As a result, modifications of the SnO2 electron transport layer led to reducing defect density and energy level mismatch, whereas the passivation of chalcogenides decreased the PbI2 residues' formation in the device structure, consequently improving efficiency and environmental stability [19]. Wang et al. analyzed the influence of N-CQDs passivation on the chalcogenides' surface defects. Analyzing interactions of the functional groups of N-CQDs with surface unsaturated sites, the authors proved the carrier complexation inhibition, which was accompanied by enhanced charge transfer across interfaces and the increase in device conversion efficiency [20]. In their paper, Guan et al. synthesized N-CQDs using walnut shell wastes and analyzed their ability to be added to the electron-transport layer with the involvement of nitrogen/oxygen-based functional groups. The obtained data confirmed increased crystallinity and lower defect density of chalcogenides, contributing to achieving a high efficiency in devices [21]. In their investigation of graphite/amorphous nitrogen-doped carbon dots as additive materials for chalcogenides, Collavini et al. studied structural interactions of these compounds and their ability to contribute to increased conversion efficiency and stability in chalcogenide cells [22].

Not limited to chalcogenide solar cells, nitrogen-doped carbon quantum dots (N-CQDs) have proven their versatility in improving the performance of various photovoltaic cells. Carolan et al. used a microplasma approach to synthesize N-CQDs and illustrated that their considerable nitrogen doping degree, along with quantum confinement effect, can serve the materials as photoactive agents for boosting open-circuit voltage in photovoltaic cells, thus proving their utility in developing advanced carbon quantum dot-based solar cells [23]. Shejale et al. developed N-CQDs by applying microwave-assisted pyrolysis technique and studied their photoelectric effect as sensitizers and synergistic photoactive agents in dye-sensitized solar cells. They showed that this material can significantly boost light harvesting, reduce recombination losses, and improve photovoltaic efficiency up to 8.75% owing to the favorable characteristics of the material such as high carrier mobility and tunable light response properties [24]. Riaz et al. developed graphitic nitrogen-doped CQDs for dye-sensitized solar cells' downshifting layer and concluded that UV light absorption and reduced recombination losses provided by the materials can significantly improve photovoltaic cell performance under UV radiation exposure, while also being environmentally friendly and durable [25]. Moreover, Wang et al. created "green" N-CQDs by applying pyrolysis process, examined their UV-VIS absorption, and achieved a photovoltaic efficiency of 0.79% in a quantum dot solar cell [26]. Finally, Liu et al. explored the ability of innovative N-CQDs for enhancing the efficiency of solar-thermal collectors. Specifically, they showed that especially graphitic nitrogen-doped CQDs expand the absorption spectrum, improve photothermal conversion, and demonstrate stability in a

nanofluid state [27].

Nevertheless, the drawbacks related to efficiency decay, hysteresis, and low stability are still major barriers to the application of chalcogenide photovoltaics. Nitrogen-doped carbon quantum dots (N-CQDs) among various carbon-based nanomaterials represent a promising class of materials that can be used for interfacial engineering of chalcogenide solar cells. In the current work, N-CQDs have been prepared using dried fenugreek and characterized by FTIR spectroscopy together with other methods. N-CQDs were introduced as an interfacial layer in the electron transport layer of the device. To clarify the impact of N-CQDs on device performance and reduction of hysteresis, J-V, EQE, and fluorescent spectra were measured before and after interfacial engineering. Additionally, the effect of N-CQDs on the stability of the device was assessed.

2 Experimental design

2.1 Experimental materials and equipment

2.1.1 Experimental reagents

The experimental reagents mainly consist of two parts, one is the chemical reagents required for the preparation of nitrogen-doped carbon quantum dots (N-CQDs), and the other is the chemical reagents required for the preparation of dye-sensitized solar cells (DSSCs), which are shown in Table 1.

Table 1: Main experimental reagent

Name	Specification	Name	Specification
Chitosan	Analytical purity	Sodium iodide	99%
NH_4OH	Chemical purity	Potassium iodide	Analytical purity
Anhydrous ethanol	Analytical purity	Lithium iodide	99.9%
C_2H_5OH	Analytical purity	Lithium perchlorate	99.9%
Tetran-butyl titanate	Chemical purity	Ammonium tetramethiodide	98%
H_2PtCl_6	Analytical purity	Ammonium tetrethyl iodide	98%
TiO_2	99.8%	Ammonium iodide was positive	Analytical purity
OP emulsifier	Superior purity	4-butyl pyridine	98%
N719 dye	≧99%	$NiSO_4$	Analytical purity
Iodine	Analytical purity		

2.1.2 N-CQDs preparation and characterization equipment

The experimental set-up was mainly composed of the equipment used for the synthesis and analysis of the N-CQDs, while the testing of solar cell characteristics relied mostly on the electrochemical workstation. The exact pieces of equipment used in both cases are listed in Table 2 below.

Table 2: Specific equipment and performance characterization equipment

Preparation instrument		Performance characterization equipment	
Instrument		Test equipment	
Hydrothermal reactor	XJ-60 ml	XRD	UitimaIV
Electric drum drying box	DGG-9030AL	Raman	In Via Cofocal micromite
Ultrasonic cleaning machine	KM-1030B	UV-vis	UV-3600
Magnetic stirrer	CJJ-781	PL	F-4500
Agate mortar	50mm	FTIR	EQUINOX 55
Centrifuge	TGL-16C	XPS	PHI500
Dialysis bag	MD45 1000D	TEM	Tecnai G2 F30
Filter film	0.22μm	Electrochemical workstation	CHI660E

2.2 Electrode Preparation

2.2.1 Preparation of N-CQDs

Firstly, the washed fenugreek was put into the oven at 65 degrees to dry, secondly, it was mashed with a glass rod, and then ground into powder with a mortar and pestle into a beaker for use. Weigh 0.35g of fenugreek powder into the reaction kettle, add 80mL of pure water, mix well and encapsulated into the oven, water-heated for 7 hours, the temperature was 110. The above compound was then heated in an oven at temperatures of 140, 170, and 210 °C for 7 hours. The reaction flask was then cooled, and the obtained liquid was filtered using filter paper, spun at 12,500 rpm for 9 minutes, and then dialyzed to eliminate impurities. This resulted in the carbon quantum dots solution.

2.2.2 Preparation of photoanode TiO_2

TiO_2 colloidal film was deposited on the cleaned FTO conductive glass by scraping coating method, and its thickness was about 10.5 μm, and the area was about 0.6×0.6 cm^2, and the area of FTO conductive glass was about 2.2×2.2 cm^2; the conductive glass coated with TiO_2 colloidal film was put into a muffle furnace to be baked, and the temperature was set at 460 ℃, and the baking time was 28 min; natural After cooling down, the synthesized TiO_2 photoanode was taken out and put into the prepared carbon quantum dot solution, and the carbon quantum dot-sensitized TiO_2 photoanode was taken out after immersion and adsorption for 25 h. The TiO_2 photoanode was blown dry with nitrogen gas, and then left to be used.

2.3 Characterization of materials and films

(1) Ultraviolet-visible absorption spectrum

UV-visible spectra used in this research were obtained through a UV-visible spectrophotometer (UV-3101 PC). The absorption phenomenon entails the absorption of ultraviolet and visible rays by molecules or ions leading to the excitation of the valence electrons. This phenomenon is mainly described by two values, that is, wavelength of the maximum absorption and the absorbance. Maximum wavelength represents the wavelength of absorption while absorbance represents the amount of light absorbed when the rays pass through the material. UV-visible spectroscopy technique is useful in measuring the absorption coefficient and optical band gap, evaluating crystal quality, and examining the composition properties of thin film chalcogenides. Transmission spectra offer data on optical properties of the transport layer.

(2) X-ray diffraction

X-ray diffraction patterns used to study the structural characteristics of thin films have been taken using the X-ray diffractometer. This is because diffraction occurs due to the interference between the waves scattered by the atoms, and such diffraction patterns provide an insight into the atomic arrangement inside the material. Analysis of XRD provides valuable insights about peak position and intensity, and consequently the nature of composition, orientation, and crystallinity.

(3) Scanning Electron Microscope

For the analysis of the surface features of the thin films in this study, scanning electron microscopy was performed. A field emission scanning electron microscope running on secondary electron mode was used in order to generate high-quality images from the scanning of an electron beam across the sample surface.

(4) Atomic force microscope

Surface roughness analysis of the fabricated thin films was done using an Atomic Force Microscope (Asylum Research Cypher S). This technique is based on the van der Waals forces between the sample and the probe tip. Surface roughness was obtained directly through the 3D plots obtained from the AFM scans.

(5) Steady-state and transient fluorescence spectroscopy

In this thesis, the steady-state fluorescence spectra of thin films were characterized by a fluorescence spectrometer modeled as Nanolog FL3-2iHR from Horiba; the transient fluorescence spectra of thin films were characterized by a transient spectrometer modeled as Delta flex from Horiba, which was excited at 530 nm with a semiconductor laser and monitored at 805 nm.

The PL and TRPL spectra allow the analysis of the luminescence peak position, luminescence peak intensity, and the change of fluorescence with time under specific wavelength excitation, characterizing the change of the chalcogenide component, the carrier composite within the film, and the carrier lifetime.

(6) Ultraviolet electron spectroscopy

In this thesis, ultraviolet photoelectron spectroscopy (UPS) was characterized by the VGScienta R4000 UVES analysis system from Scienta Omicron, Sweden, and the excitation source used was He I. The UVES analysis was performed by the VGScienta R4000 UVES analysis system from Scienta Omicron, Sweden.

2.4 Device Test Methods

(1) Current-Voltage Characterization

The I-V curves for the device examined in the study have been acquired using a digital source meter. The digital source meter is an instrument that possesses many features including being multifunctional, accurate, and programmable, which allows it to acquire the I-V curve. In addition, it can measure variations in the voltage and current.

(2) Solar light source simulator

The solar light source simulator of this thesis provides the solar spectrum.

(3) Photocurrent response spectrum

The solar cell spectral responsivity measurement system is used to characterize the external quantum efficiency of the device in this thesis.

(4) AC Impedance Spectrometer

The impedance of the devices in this thesis is analyzed and measured using an AC impedance spectrometer and is done under dark field conditions.

2.5 Battery performance parameters

Solar cell performance parameters include V_{OC}, J_{SC}, FF and PCE.

Open-circuit voltage: solar cells in the standard light source irradiation, without any external load, the battery voltage measured at both ends.

Short-circuit current: solar cells in the standard light irradiation, closed loop in the case of short-circuit current.

Filling factor: the ratio of the maximum output power to the product of open circuit voltage and short circuit current.

$$FF = \frac{V_m J_m}{V_{OC} J_{SC}} \tag{1}$$

where V_m is the voltage at the maximum power point and J_m is the current at the maximum power point. FF is an important indicator of solar cell output characteristics.

Power Conversion Efficiency:The PCE is defined as the ratio of the maximum output power of the solar cell to the incident power received by the cell surface, and can be expressed as:

$$PCE = \frac{P_m}{P_{in}} = \frac{V_{OC} J_{SC} FF}{P_{in}} \tag{2}$$

where P_m is the maximum output power and P_{in} is the power incident on the cell surface.

3 Experimental results and discussion

3.1 Characterization results and analysis of N-CQDs

3.1.1 Morphological and dimensional analysis of N-CQDs

The morphological structure, particle size, and dispersion behavior of nitrogen-doped carbon quantum dots (N-CQDs) were investigated using TEM imaging techniques. Figure 1 presents the images of TEM together with their particle size distribution curves showing that the shape of particles is roughly spherical with uniform dispersion. The size distribution of particles can be observed from Fig. 1(a) and (b), where the images of TEM and the particle size distribution curve are shown, respectively. From the fitted curve, the average particle size was obtained to be 2.98 ± 0.11 nm.

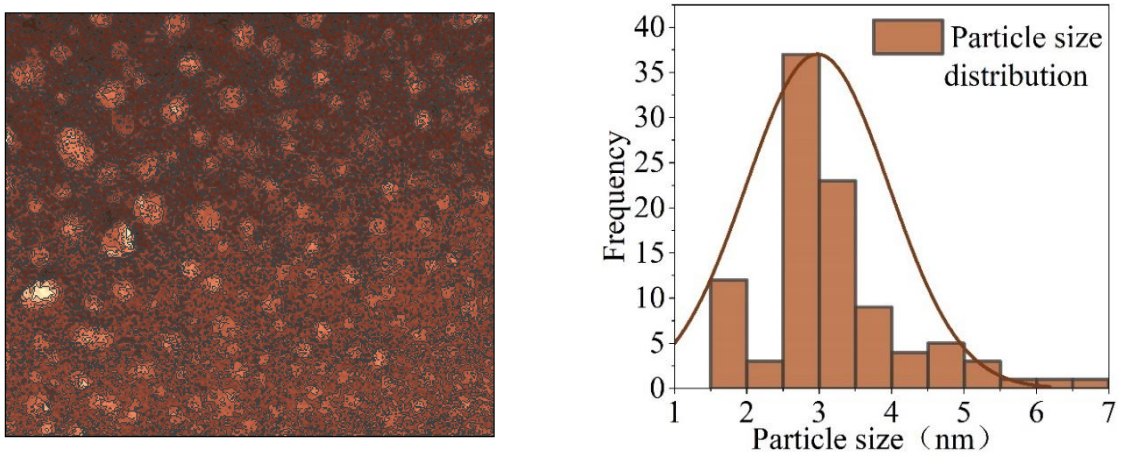

(a) TEM image (b) Particle size distribution

Figure 1: TEM and particle size distribution

3.1.2 FTIR spectral analysis of N-CQDs

FTIR spectra for the N-CQDs are provided in Figure 2. The band appearing at 1420 cm^{-1} is due to stretching vibration of C=O in -COOH, whereas that appearing at 1125 cm^{-1} is due to bending vibration of C-O. The band at 943 cm^{-1} is attributed to deformation vibration of hydroxyl group, and the band at 642 cm^{-1} is due to C-N stretching. Besides, bands at 3230 cm^{-1} and 2650/2250 cm^{-1} are due to O-H and C-H stretching, respectively. This shows that there are OH, COOH, and NH functionalities present on the surface of prepared N-CQDs. The presence of many hydrophilic groups gives the synthesized material good water solubility. From the perspective of excitation radiative recombination process, a good electron-donating ability of the surface group plays an important role in providing electrons. Therefore, the presence of OH and NH groups enhances fluorescence emission of the N-CQD.

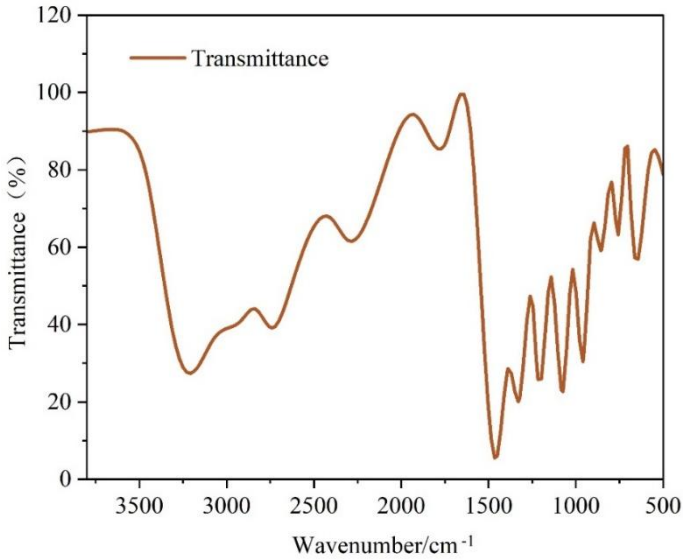

Figure 2: The infrared spectrum of the N-CQDs

3.1.3 UV-Vis absorption spectroscopy of N-CQDs

The characterization for UV–Vis was done by dispersing N-CQDs in ethanol and placing them

in a two-faced transparent cuvette; results of which have been given in Fig. 3. The material shows a wide absorption curve in the region of 280-600 nm with the main absorption peak at 352 nm that may be due to the transition between n-π* related to C=O bonds in the carboxyl group of N-CQDs. After 410 nm, the absorbance decreases gradually with respect to wavelength, and above 620 nm absorbance is minimal.

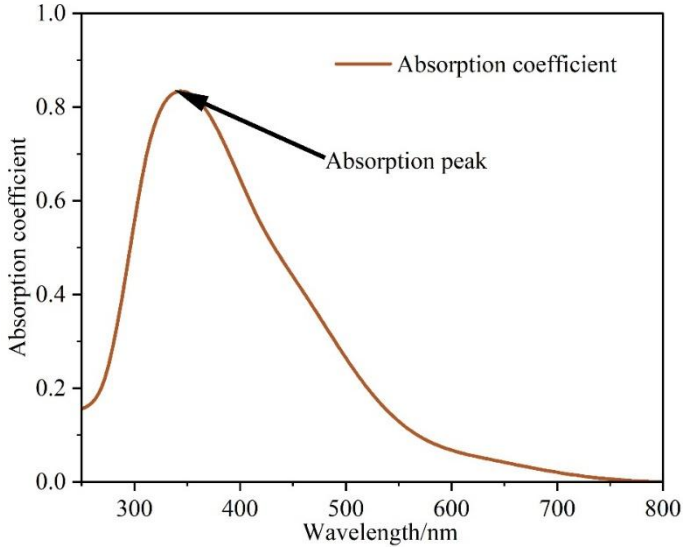

Figure 3: Dispersed absorption spectra in ethanol

3.1.4 Fluorescence emission spectroscopy of N-CQDs

To study the optical properties of nitrogen-doped carbon quantum dots (N-CQDs), these nanoparticles were dispersed in anhydrous ethanol solution, then the particles were loaded into a quartz cuvette having four optically transparent surfaces. The fluorescence experiments were performed using various excitation wavelengths. The spectra corresponding to the different excitation wavelengths are shown in Fig. 4. As observed from the figure, there is strong dependence of emission spectrum with respect to excitation wavelength for N-CQDs. With an increase in the excitation wavelength from 370 to 520 nm by 10 nm intervals, a red shift in the emission peaks occurred from 498 to 550 nm. Furthermore, the intensity of the emission also showed initial increase followed by decrease and reached its maximum value for an excitation wavelength of 480 nm with an emission peak wavelength of 538 nm. The result is consistent with those reported earlier for carbon quantum dots. Though the exact mechanism for excitation wavelength-dependent emission is not yet known, however, two plausible mechanisms which have been considered before are that: (i) variation in the size of particles and (ii) variation in the number and density of emissive sites on carbon quantum dots.

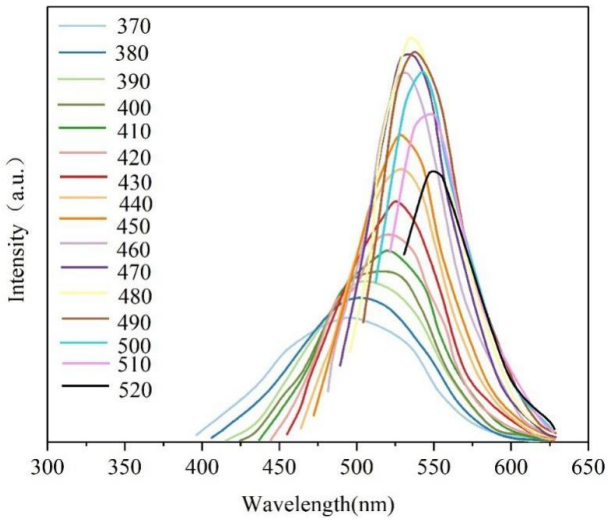

Figure 4: The emission spectrum of N-CQDs under different wave wavelengths

3.2 Electrochemical performance of nitrogen-doped carbon-modified chalcogenide cells

3.2.1 Carrier Transport and Compounding

For evaluating the influence of N-CQDs as interfacial modifiers on the carrier recombination performance, photoluminescence (PL) and time-resolved photoluminescence (TRPL) spectra of chalcogenide films were determined, where the relevant curves have been shown in Figure 5. The excitation source was a laser with an excitation wavelength of 530 nm. As can be observed from Figure 5(a), the photoluminescence intensity of the chalcogenide film deposited on TiO_2/N-CQDs substrate decreased compared to that of the pristine sample, implying better efficiency in charge transfer in the presence of N-CQDs.

In order to verify if N-CQDs improve interfacial coupling between TiO_2 and chalcogenide film, current-voltage (J-V) measurements were performed for devices prepared under light intensity from 40 to 120 mW cm^{-2}, followed by analyzing the Jsc and Voc dependence on illumination intensity I. The Jsc versus light intensity plot is shown in Figures 5(b) and 5(c). An increase in light intensity results in an increase in Jsc value, and the slope of Jsc versus light intensity was found to be 0.275 for the modified device while 0.215 for the bare device, indicating that N-CQDs reduce nonradiative recombination. The slopes of Voc plotted against light intensity were calculated to be 1.57 k_BT/q and 1.46 k_BT/q for the modified and unmodified devices, respectively. Moreover, the ideality factor of the modified device was close to unity.

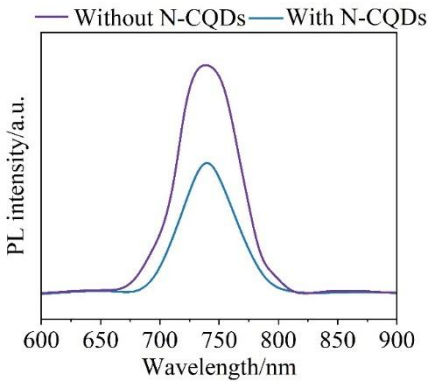

(a) PL spectrum

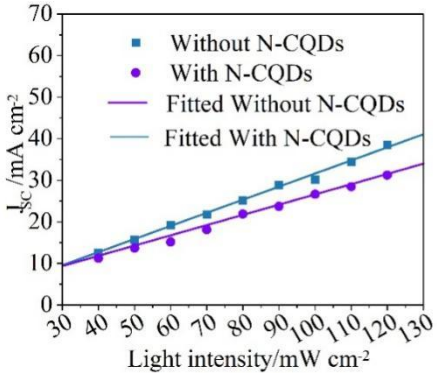

(b) JSC transform curve

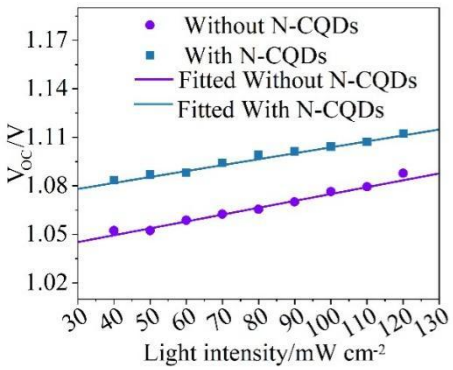

(c) VOC transform curve

Figure 5: The effect of the N-CQDs on the composite dynamics of the carrier

3.2.2 Electrochemical performance testing

Electrochemical properties of the prepared samples have been studied and are illustrated in Fig. 6, whereas the photovoltaic characteristics of treated and untreated cells are compared in Fig. 6(a). In particular, for the pristine cell, the short circuit current density Jsc equaled 26.22 mA cm^{-2}, while the open circuit voltage Voc equaled 1.045 V. Upon N-CQD incorporation, the short-circuit current density Jsc increased to 27.13 mA cm^{-2}, and the open-circuit voltage Voc reached 1.115 V. This can be explained by the changes in energy levels of TiO2 caused by N-CQDs, as well as the fact that quantum dots have a dual effect in passivating defects at the TiO2/chalcogenide interface, thus increasing the efficiency of electron transfer due to the improved alignment of energy levels of TiO_2 and the chalcogenide semiconductor. Moreover, N-CQDs can passivate defects at the TiO_2/calcite interface, therefore decreasing non-radiative recombination.

Figure 6(b) shows EQE spectra for the fabricated solar cell within the wavelength range of 300 - 1000 nm. In accordance with data from Fig. 6(b), the integrated current for the modified device is 23.94 mA cm^{-2}, which is higher than that of the pristine device (21.89 mA cm^{-2}) and correlates with the increase in the short-circuit current density.

The overall impact of incorporating N-CQD into the solar cell structure was assessed through calculating the PCE for 70 devices produced in one batch in similar conditions, including those with the modification and the control sample. The results of statistical analysis are demonstrated in Fig. 6(c). The mean PCE was calculated for 70 devices and amounted to 16.54% for the control sample and 20.34% for the treated cells.

Finally, the effect of N-CQD modification on the stability of solar cells was evaluated by storing fabricated devices in ambient conditions for 600 hours at humidity levels of 21% - 31%. PCEs of both kinds of devices were monitored during this period, and the results are illustrated in Fig. 6(d). After 600 h, the PCE of the untreated device decreased to 56.32% of its initial value, whereas that of the modified device equaled 94.12%. It is due to the hydrophobic property of N-CQDs..

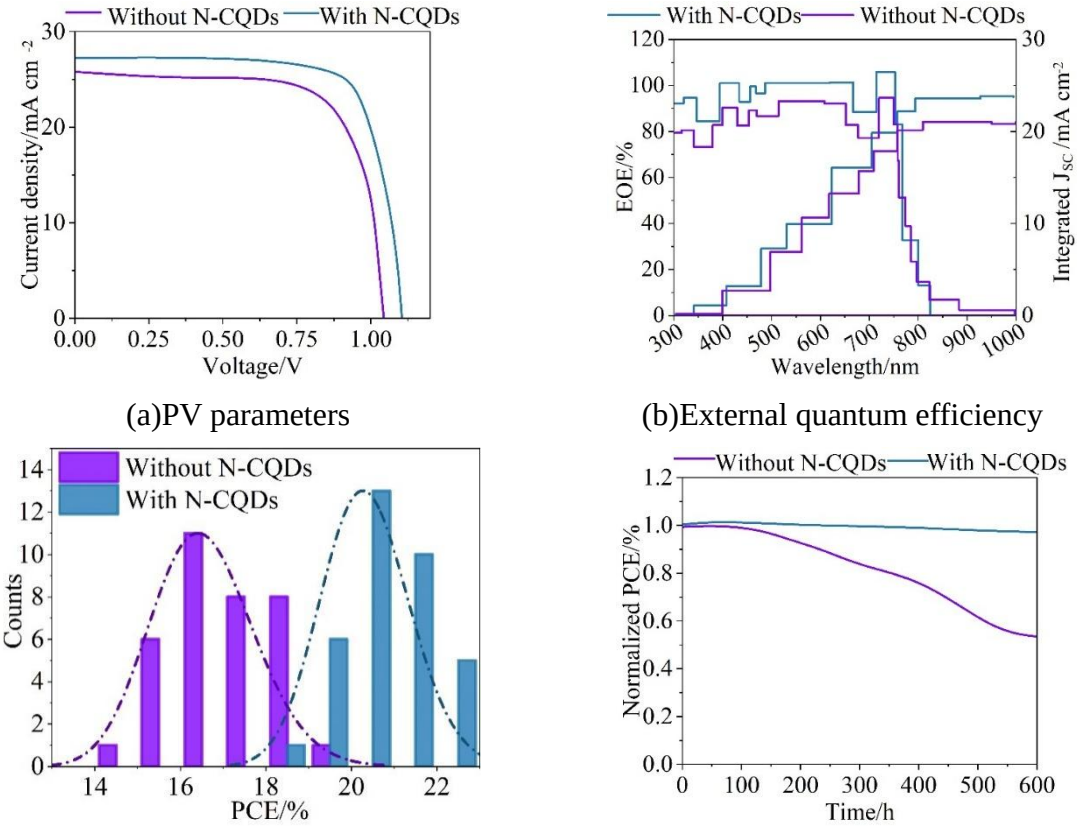

(a)PV parameters (b)External quantum efficiency

(c)PCE statistics (d)Normalized PCE curve

Figure 6: Electrochemical performance test

3.3 Performance analysis of nitrogen-doped carbon-modified chalcogenide cells

3.3.1 Effect of nitrogen-doped carbon on the physical properties of chalcogenides

Theoretically a larger contact area means that there can be more electron transport through the N-CQDs, and the carrier lifetime can be increased due to the reduction of the number of defects at the interface which also results in a reduction of the number of carriers being complexed, in order to validate this idea, we have performed PL and TRPL tests, the results of which are shown in Fig. 7.

Samples for the current experiments represent films made of chalcogenides with and without the use of nitrogen-doped carbon quantum dots (N-CQDs). Contrary to the previously performed study, the steady-state PL measurements carried out within this experiment serve to evaluate carrier-extraction efficiency because low PL values suggest an efficient extraction of carriers from the film. The differences in PL spectra of chalcogenide films with and without N-CQDs can be seen in Figure (a), in which one may observe that the film consisting solely of chalcogenides shows higher values than that containing CQDs. This suggests that the addition of CQDs increases carrier quenching and extraction. Moreover, TRPL analysis was also performed to find out whether carbon quantum dots affect the lifetime of nonequilibrium carriers in chalcogenide films. The samples analyzed in this case are the same as those used for the steady-state PL measurements. So the double exponential function is used for fitting, the specific parameters of TRPL fitting are shown in Table 3, the fitting results in the fast decay time of 10.03ns and 14.65ns for doped and undoped samples, respectively, and the slow decay

process of 20.85ns and 128.66ns, and the increase in fluorescence lifetime indicates the decrease of non-radiative compounding, which is beneficial for device efficiency. This facilitates the improvement of device efficiency, while the combined PL and TRPL results also indicate that more favorable film surface contact can also lead to better carrier transport properties.

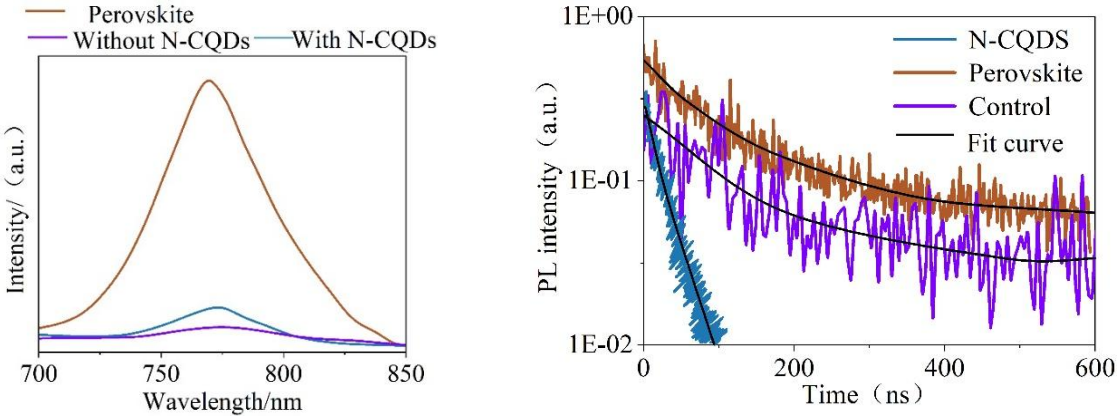

(a) PL map (b) TRPL map

Figure 7: The PL map and the TRPL map

Table 3: The TRPL is fitted with specific parameters

	Fast decay time (τ1/ns)	A1/%	Slow decay time (τ2/ns)	A2/%	τavg/ns
Undoped N-CQDs	14.65	24.56	128.66	75.48	100.71
N-CQDs	10.03	20.32	20.85	79.62	18.75
Perovskite	245.44	21.58	1307.64	78.42	1079.54

3.3.2 Effect of Nitrogen-Doped Carbon on Device Stability of Cells

For the chalcogenide battery is always a difficult to bypass the topic, which is also particularly important for the future commercialization of chalcogenide devices, so we tested the stability of the device accordingly, chalcogenide battery stability decay map and Ag electrode surface GIXRD pattern shown in Figure 8. The optimal efficiency of the doped and undoped devices was selected for the test, and in order to more closely match the actual device placement and preservation scenarios, we chose to carry out the test in an ordinary environment of the drying box rather than a glove box, and the test time of the device was 4 weeks, and the stability of the calixarene battery decay graph is shown in Figure (a), the efficiency of the doped device is maintained at 62%, whereas the efficiency of the un-doped device is only 11%, which indicates that doping of carbon quantum dots has a very significant effect on improving the stability of devices. This shows that the doping of carbon quantum dots has a very obvious effect on the stability of the device, by observing the device after placement we found that the Ag electrode of the doped cell is relatively well preserved, while the electrode of the un-doped device is obviously corroded phenomenon, we guess that it is due to the decomposition of the calixarene which leads to the reaction of iodine ions with the Ag electrode, in order to verify the conjecture, we carried out the GIXRD test on the surface of the Ag electrode after placement. Compared with normal XRD, GIXRD can obtain more surface phase information of the material, which is very suitable for the silver electrode with small thickness. The results of the GIXRD mapping of the Ag electrode surface are shown in Fig. (b), and it is found that the electrode of the un-doped sample placed for a long time has generated AgI, which shows that the decomposition

of chalcocite has already occurred, resulting in a rapid decrease in the efficiency of the un-doped sample. For the inner process that carbon dots can slow down the decomposition of chalcogenides because it is more difficult to be observed directly, so we made a conjecture: on the one hand, free iodine ions and lead ions in chalcogenides will combine with carbon quantum dots to form intermediate adducts, preventing iodine ions from diffusing through the N-CQDs to generate AgI, and ensuring that the electrodes can continue to work; on the other hand, there are also some water-resistant groups in carbon quantum dots. On the other hand, there are some water-resistant groups in carbon quantum dots, such as -CH2-, C=C, C=O, these groups can prevent the decomposition of water for the chalcogenide film to a certain extent, and the above two doped devices have 51% stability improvement compared to the undoped ones.

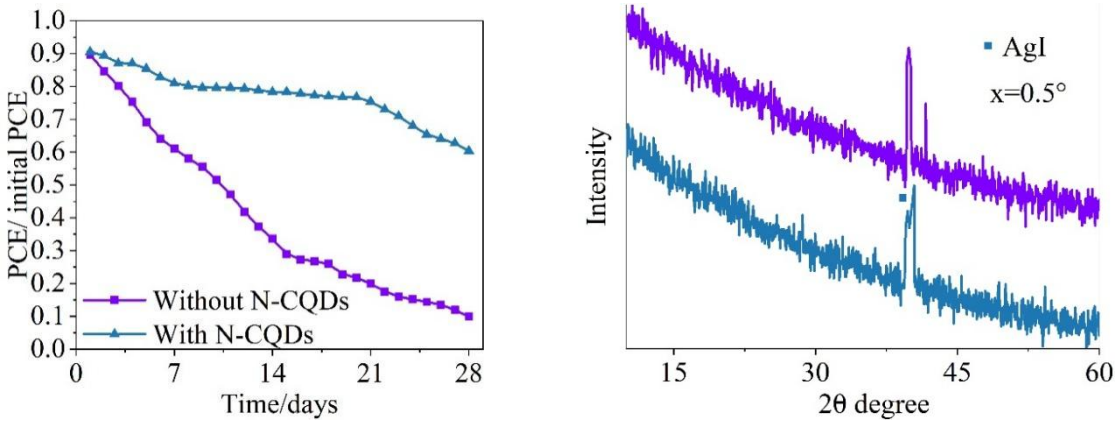

(a)Stability attenuation (b)GIXRD map

Figure 8: Battery stability attenuation and electrode surface GIXRD map

4 Conclusion

The correlation analysis between Fourier transform infrared spectroscopy, UV-vis spectroscopy, and fluorescence emission spectroscopy in this work indicated that N-CQDs possess suitable energy levels, good light harvesting properties, and abundant surface functional groups (especially C=O and C-O). Such physicochemical properties render N-CQDs useful for the modification at interfaces.

After the introduction of N-CQDs at interfaces, the integrated current density was increased from 21.89 mA cm^{-2} to 23.94 mA cm^{-2}, and the photovoltaic power conversion efficiency was improved to 20.34%. Moreover, the ideality factor was close to unity. Therefore, N-CQDs can effectively decrease the non-radiative recombination rate and increase charge collection efficiency.

In addition, the interfacial modification decreased hysteresis significantly. As we all know, such modifications can improve energy-level alignment and charge-transfer dynamics of the interface, reduce the density of defects in the interfacial region as well as the formation of complex carriers, and increase carrier lifetime, thus reducing hysteresis.

According to GIXRD and time-resolved fluorescence analysis, N-CQDs could react with the free iodides in calixarene molecules, forming a stable intermediate. Such reactions can decrease iodide migration and calixarene decomposition effectively. Meanwhile, N-CQDs can prevent water infiltration due to their hydrophobicity, resulting in a 51% improvement in stability of the modified device.

Through the synergistic effect of multiple mechanisms such as defect passivation, ion migration inhibition and interfacial protection, N-CQDs show significant advantages in

enhancing the efficiency, stability and reducing the hysteresis effect of chalcogenide solar cells, and the N-CQDs materials have important application prospects in the optimization of different device structures.

About the Author

Xiaolin Wang (1980–), female, Han nationality, native of Anshan, Liaoning, Ph.D., major research fields: Materials Science, Novel Energy Materials.

References

[1] Li, X., Yan, L., Ding, C., Song, H., Yang, Y., & Ma, C. Q. (2022). Carbon dots in perovskite solar cells: properties, applications, and perspectives. Energy & Fuels, 37(2), 876-901.

[2] Kim, J. Y., Lee, J. W., Jung, H. S., Shin, H., & Park, N. G. (2020). High-efficiency perovskite solar cells. Chemical reviews, 120(15), 7867-7918.

[3] Rong, Y., Hu, Y., Mei, A., Tan, H., Saidaminov, M. I., Seok, S. I., ... & Han, H. (2018). Challenges for commercializing perovskite solar cells. Science, 361(6408), eaat8235.

[4] Shao, S., & Loi, M. A. (2020). The role of the interfaces in perovskite solar cells. Advanced Materials Interfaces, 7(1), 1901469.

[5] Ball, J. M., & Petrozza, A. (2016). Defects in perovskite-halides and their effects in solar cells. Nature Energy, 1(11), 1-13.

[6] Fang, Z., Sun, J., Liu, S. F., & Ding, L. (2023). Defects in perovskite crystals. Journal of Semiconductors, 44(8), 080201.

[7] Dsouza, S. D., Buerkle, M., Brunet, P., Maddi, C., Padmanaban, D. B., Morelli, A., ... & Svrcek, V. (2021). The importance of surface states in N-doped carbon quantum dots. Carbon, 183, 1-11.

[8] Travlou, N. A., Giannakoudakis, D. A., Algarra, M., Labella, A. M., Rodríguez-Castellón, E., & Bandosz, T. J. (2018). S-and N-doped carbon quantum dots: Surface chemistry dependent antibacterial activity. Carbon, 135, 104-111.

[9] Xu, T., Wan, Z., Tang, H., Zhao, C., Lv, S., Chen, Y., ... & Huang, W. (2021). Carbon quantum dot additive engineering for efficient and stable carbon-based perovskite solar cells. Journal of Alloys and Compounds, 859, 157784.

[10] Lim, S. Y., Shen, W., & Gao, Z. (2015). Carbon quantum dots and their applications. Chemical Society Reviews, 44(1), 362-381.

[11] Das, R., Bandyopadhyay, R., & Pramanik, P. (2018). Carbon quantum dots from natural resource: A review. Materials today chemistry, 8, 96-109.

[12] Tian, L., Li, Z., Wang, P., Zhai, X., Wang, X., & Li, T. (2021). Carbon quantum dots for advanced electrocatalysis. Journal of Energy Chemistry, 55, 279-294.

[13] Wang, Y., & Hu, A. (2014). Carbon quantum dots: synthesis, properties and applications. Journal of Materials Chemistry C, 2(34), 6921-6939.

[14] Shen, D., Lan, T., Qiao, D., Guo, M., Zuo, J., Gu, S., ... & Wei, M. (2024). Tunable photoluminescent nitrogen-doped graphene quantum dots at the interface for high-efficiency perovskite solar cells. ACS Applied Nano Materials, 7(2), 2232-2243.

[15] Wen, Y., Zhu, G., & Shao, Y. (2020). Improving the power conversion efficiency of perovskite solar cells by adding carbon quantum dots. Journal of Materials Science, 55(7), 2937-2946.

[16] Peng, W., Li, S., Li, M., Chen, M., & Yang, Y. (2022). Enhancement of the electron transportation in the perovskite solar cells via optimizing the photoelectric properties of electron transport layer with nitrogen-doped graphene quantum dots. Journal of Materials Science: Materials in Electronics, 33(18), 14443-14456.

[17] Riaz, S., & Park, S. J. (2022). Thioacetamide-derived nitrogen and sulfur co-doped carbon quantum dots for “green” quantum dot solar cells. Journal of Industrial and Engineering Chemistry, 105, 111-120.

[18] Kırbıyık, Ç., Toprak, A., Başlak, C., Kuş, M., & Ersöz, M. (2020). Nitrogen-doped CQDs to enhance the power conversion efficiency of perovskite solar cells via surface passivation. Journal of Alloys and Compounds, 832, 154897.

[19] Li, C., Yao, D., Dong, P., Tang, Z., Li, Y., Chen, B., ... & Long, F. (2024). Synergetic modification on buried and upper surfaces of perovskites with nitrogen-doped carbon quantum dots for efficient and stable solar cells. Applied Surface Science, 658, 159848.

[20] Wang, Y., Zhang, J., Chen, S., Zhang, H., Li, L., & Fu, Z. (2018). Surface passivation with nitrogen-doped carbon dots for improved perovskite solar cell performance. Journal of Materials Science, 53(12), 9180-9190.

[21] Guan, H. Y., Lei, Y. L., Chen, Q., Ding, J., Lei, H. W., Guo, Y. X., ... & Xiang, F. (2022). Synthesis of Nitrogen-Doped Carbon Quantum Dots from Walnut Shell Waste as Electron Transport Layer Additive for Perovskite Solar Cells. Journal of Nano Research, 76, 49-60.

[22] Collavini, S., Amato, F., Cabrera-Espinoza, A., Arcudi, F., Đorđević, L., Kosta, I., ... & Delgado, J. L. (2022). Efficient and Stable Perovskite Solar Cells based on Nitrogen-Doped Carbon Nanodots. Energy Technology, 10(6), 2101059.

[23] Carolan, D., Rocks, C., Padmanaban, D. B., Maguire, P., Svrcek, V., & Mariotti, D. (2017). Environmentally friendly nitrogen-doped carbon quantum dots for next generation solar cells. Sustainable Energy & Fuels, 1(7), 1611-1619.

[24] Shejale, K. P., Jaiswal, A., Kumar, A., Saxena, S., & Shukla, S. (2021). Nitrogen doped carbon quantum dots as Co-active materials for highly efficient dye sensitized solar cells. Carbon, 183, 169-175.

[25] Riaz, R., Ali, M., Maiyalagan, T., Anjum, A. S., Lee, S., Ko, M. J., & Jeong, S. H. (2019). Dye-sensitized solar cell (DSSC) coated with energy down shift layer of nitrogen-doped

carbon quantum dots (N-CQDs) for enhanced current density and stability. Applied Surface Science, 483, 425-431.

[26] Wang, H., Sun, P., Cong, S., Wu, J., Gao, L., Wang, Y., ... & Zou, G. (2016). Nitrogen-doped carbon dots for “green” quantum dot solar cells. Nanoscale research letters, 11(1), 27.

[27] Liu, Y., Dong, C., Peng, C., Zhang, T., & Zhang, L. (2024). Nitrogen-doped carbon quantum dots enable efficient photothermal conversion for direct absorption solar collectors. Solar Energy Materials and Solar Cells, 278, 113178.